Preprint Cambridge Centre for Computational Chemical Engineering ISSN 1473 – 4273

Modelling soot formation from wall films in a gasoline direct injection engine using a detailed population balance model

Buyu Wang [1], Sebastian Mosbach [2], Sebastian Schmutzhard [2],
Shijin Shuai [1], Yaqing Huang [1], Markus Kraft [2,3]

released: 19 June 2015

[1] Department of Automotive Engineering
Tsinghua University
Haidian District
Beijing, 100084
China
E-mail: sjshuai@tsinghua.edu.cn

[2] Department of Chemical Engineering
and Biotechnology
University of Cambridge
New Museums Site
Pembroke Street
Cambridge, CB2 3RA
United Kingdom

[3] School of Chemical
and Biomedical Engineering
Nanyang Technological University
62 Nanyang Drive
Singapore 637459
E-mail: mk306@cam.ac.uk

Preprint No. 157

Keywords: GDI engine, soot, wall film

Edited by
Computational Modelling Group
Department of Chemical Engineering and Biotechnology
University of Cambridge
New Museums Site
Pembroke Street
Cambridge CB2 3RA
United Kingdom

Fax: + 44 (0)1223 334796
E-Mail: c4e@cam.ac.uk
World Wide Web: http://como.cheng.cam.ac.uk/

Abstract

In this study, soot formation in a Gasoline Direct Injection (GDI) engine is simulated using a Stochastic Reactor Model (SRM Engine Suite) which contains a detailed population balance soot model capable of describing particle morphology and chemical composition. In order to describe the soot formation originating from the wall film, the SRM Engine Suite is extended to include spray impingement and wall film evaporation models. The cylinder is divided into a wall and a bulk zone to resolve the equivalence ratio and temperature distributions of the mixture near the wall. The combustion chamber wall is assumed to exchange heat directly only with the wall zone. The turbulent mixing within each zone and between the two zones are simulated with different mixing models. The effects of key parameters on the temperature and equivalence ratio in the two zones are investigated. The mixing rate between the wall and bulk zone has a significant effect on the wall zone, while the mixing rate in the wall zone only has a negligible impact on the temperature and equivalence ratio below a certain threshold. Experimental data are obtained from a four-cylinder, gasoline-fuelled direct injection spark ignition engine operated stoichiometrically. An injection timing sweep, ranging from 120 CAD BTDC to 330 CAD BTDC, is conducted in order to investigate the effect of spray impingement on soot formation. The earliest injection case (330 CAD BTDC), which produces significantly higher levels of particle emissions than any other case, is simulated by the current model. It is found that the in-cylinder pressure and the heat release rate match well with the experimental data. The particle size distribution in the simulation has the same order of magnitude as the experimental one. By tracing the particles in an equivalence ratio-temperature diagram, it is demonstrated that the rich mixture near the wall becomes the source of the soot formation as a result of the wall film evaporation.

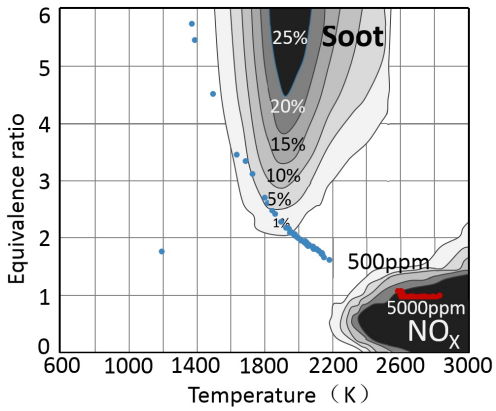

- Soot formation from a wall film in a GDI engine is simulated.
- Spray impingement and wall film evaporation models are added to SRM Engine Suite.
- Soot is modelled using a highly detailed population balance model.
- Particle size distributions are measured experimentally.
- Evolution of wall region is shown in equivalence ratio-temperature diagrams.

Contents

1 Introduction

Gasoline Direct Injection (GDI) engines are becoming the most widely used gasoline engines all over the world attributed to the high efficiency compared with traditional Port Fuel Injection (PFI) engines [55]. Unfortunately, the particle emissions are higher for GDI engines, and it is difficult for the manufacturers to control the particle mass and number below the limit value of EURO VI ($\mathrm{PM} < 5$ mg/km and $\mathrm{PN} < 6 \times 10^{11}$ particles/km) [7, 43, 61]. Additionally, the fine particles, especially the ones with the size less than 2.5 μm (known as PM2.5), have adverse health effects [48]. Thus, it is necessary to determine the source of particles in GDI engines and take measures to reduce the particle emissions.

It is well-known that the engine-out particulate matter from Diesel engines can be divided into two modes by size, the nucleation mode and the accumulation mode [26]. For the nucleation mode, the particles normally have the size ranging between 5 and 50 nm and consist of soluble organic fraction (SOF) and sulfate. Typically the nucleation mode contains 1-20% of the particle mass and more than 90% of the particle number. For the accumulation mode, main part of the particles is dry soot with the size ranging between 100 to 300 nm. It was found by many tests that most of the particles from GDI engines are located in the accumulation mode [7, 19, 61]. The peak value of the accumulation mode is around 100 nm.

Because of the longer ignition delay and good volatility of gasoline, fuel in GDI engines has sufficient time to premix and fewer locally fuel-rich regions are formed than in compression ignition direct injection (CIDI) engines, especially if the injection takes place long before top dead center. So the traditional soot formation mechanism may not be applicable for GDI engines. The soot formation process in GDI engines has been widely investigated by optical methods such as high-speed camera combustion images [8, 16, 74], two colour method [64], Laser-Induced Fluorescence (LIF) [45, 63] and Laser-Induced Incandescence (LII) [54, 70]. Wyszyński et al. [74] compared three fuels (unleaded gasoline, *iso*-octane, and toluene) on an optical GDI engine. From high-speed combustion images, they observed soot formed in rich regions from pool fires glowing late in the engine cycle. Catapano et al. [8] also used combustion images of ethanol and gasoline blends to demonstrate that the diffusion combustion of fuel films is the source of soot formation. Similar results were found by Fatouraie et al. [16]. Stojkovic et al. [64] used two colour method to calculate the soot concentration in a stratified charge GDI engine and described the soot formation in detail. They concluded that there are two main sources of soot formation: one is the partially premixed flame through locally rich zones and the other is pool fires fed by piston surface films. Soot from the former burns out rapidly due to high temperature and rapid mixing with surrounding lean regions, while soot from the latter can persist until late in the cycle, when soot oxidation is unlikely as a result of low temperature and vanishing hydroxyl radicals. Recently, Rossbach et al. [54, 70] used LII to quantify soot formation in a Direct Injection Spark Ignition (DISI) engine. They measured the soot concentrations, mean particle diameters and number densities in different combustion modes and different injection timings. Besides, Berndorfer et al. [5] proposed that another source for soot in GDI engines might be the diffusion flame near the tip of the injector. The soot emissions can be worse for a coked injector. The liquid fuel film

wetting the piston surface is at relatively low temperature, evaporates and is subject to slow oxidation – such conditions trigger the formation of carbonaceous deposits [20, 32]. The resulting coke coating decreases the thermal conductivity of the walls and thus leads to increased operating temperature in the engine [33]. Fuel can condense in the porous deposit during the injection and be released at the end of the power stroke, causing increased emission of soot [49]. The deposits formed at the injector nozzles can seriously affect their performance [20]. The processes of deposit and soot formation are conjugated – soot may nucleate or sediment onto deposit contributing to its thickness, and vice versa, engine deposits may significantly alter the soot emissions [20, 32]. In summary, numerous studies demonstrate that the wall film formed due to spray impingement is the main source of soot and carbonaceous deposits in GDI engines.

Even though there are many numerical works focused on soot formation and oxidation in Diesel engines, computational research into GDI soot formation is currently very limited, especially studies considering both the detailed wall film formation and soot formation. Etheridge et al. [13] coupled Stochastic Reactor Model (SRM) with SWEEP, a Monte Carlo based population balance solver, to simulate the soot formation in a stratified charge GDI engine and found the high stratification by late injection led to more soot emissions. Jiao and Reitz [23] and Naik et al. [42] performed 3D computational fluid dynamics simulations in GDI engines to show the in-cylinder soot evolution by semi-detailed soot models. But none of them considered the effect of spray impingement and soot from the wall film. Sukegawa et al. [68] applied LES to simulate the mixture formation process including spray development and impingement, but they did not calculate the combustion process and particle results were given by empirical expressions only.

In order to describe soot formation from the wall film, the spray impingement process and the wall film evaporation should be considered. In addition, the same processes control the temperature and the evolution of the composition of the film, which are the most important factors affecting coking [20]. Since Naber and Reitz first modelled the spray impingement [40], a number of models have been proposed. Most of the models contain three major parts: the regimes of spray impingement, the criteria for different regimes, and the calculation of the post-impingement characteristics [30]. Naber and Reitz describe three regimes: stick, reflect, and jet [40]. However, they did not provide any criteria to discriminate between the different regimes. Shih and Assanis [57] and Watkins [71, 72] respectively modified Naber model by setting the Weber number as criteria. They used different methods to calculate the droplet characteristics after impingement. Mundo et al. [38, 39] and Senda et al. [56] developed a spray-wall interaction model based on experiments and took the state of the wall into account. Based on previous research, the well-known Bai and Gosman model [1] was proposed and widely used in different engine conditions. For example, Su et al. [66] incorporated the Bai and Gosman model into a stochastic spray model to investigate the dual-injection HCCI combustion, where the first injection event of Diesel fuel at low in-cylinder pressure during compression caused impingement of the fuel on the wall. To better model gasoline spray impingement, Bai and Gosman modified the original model in 2002 [3]. More details about the Bai and Gosman model are described in the next section. Following Bai and Gosman, Stanton and Rutland [62], O'Rourke and Amsden [44], Trujillo et al. [69], Han et al. [21], Lee et al. [28, 29], and Kim et al. [25] proposed their own spray impingement models, respectively. The major differences among these models are the definition of the criteria between different

regimes and the assumptions and calculation methods used to determine the droplet speed and size distribution after impingement.

The aim of this paper is to present an engine model which can be used to simulate soot formation in a GDI engine accounting for the effect of a wall film. The model incorporates a detailed population balance soot model, which can describe the soot morphology and chemical composition, and is applied to simulate a GDI engine with an early injection and spray impingement. The paper is structured as follows. Firstly the engine and soot model details are explained. Then, the algorithm to calculate the spray impingement and film evaporation is presented. In the subsequent section, the results of numerical simulations are compared with experimental results.

2 Model description

In this section the integrated engine and soot model is briefly summarised. The modifications to this model made as part of this work, which include spray impingement, wall film evaporation, heat transfer, and mixing sub-models, are also described.

2.1 Existing model

2.1.1 Engine model

The Stochastic Reactor Model (SRM) is a spatially zero-dimensional model of the contents of the combustion chamber based on Probability Density Function (PDF) transport methods [11, 51]. The model has been successfully employed in a number of studies in Homogeneous Charge Compression Ignition (HCCI) engines [6, 27, 36, 65], Spark Ignition (SI) engines [14], conventional Compression Ignition Direct Injection (CIDI) engines [59], and Partially Premixed Compression Ignition (PPCI) engines [60]. It was also previously used to simulate soot in HCCI [37], stratified GDI [13], and conventional compression ignition engines [60]. Being a PDF method, the SRM describes distributions of temperature and species concentrations within the engine cylinder. These distributions are represented by an ensemble of stochastic particles, each of which can be thought of as a fluid parcel in the cylinder with its own temperature and composition. The time-evolution of the stochastic particles and hence the distributions as a consequence of processes such as turbulent mixing, heat transfer, direct injection, and flame propagation is described by appropriate sub-models. The number of particles governs the precision of predictions. To eliminate the dependence on the particle number, 100 particles are sufficient in many applications according to previous studies (*e.g.* [37]). An advantage of SRM is that it allows detailed chemistry calculations with relatively short computational times. In this work, a detailed Primary Reference Fuel (PRF) mechanism containing 208 species and 1002 reactions is employed [37].

2.1.2 Soot model

In order to describe the formation and oxidation of soot, a detailed set of population balance equations is solved by SWEEP [9], which is based on a Monte Carlo method [4, 18, 47].

The soot model tracks for each aggregate the surface area, the number of primary particles and the diameter of each primary particle. The numbers of carbon atoms, hydrogen atoms and PAH molecules for each aggregate are also stored to model the chemical composition of soot. By using the Aromatic Site Counting Model [10], each type of functional site on a PAH is tracked including free edge, armchair, zigzag, and bay sites, and five-membered rings. A statistical representation of the functional sites on the PAHs is employed instead of tracking each molecule in order to achieve acceptable computational times and memory requirements. Since tracking such a large number of quantities results in a very high-dimensional population balance, a Monte Carlo method is used to solve it – being the only method suitable to treat such problems.

In terms of processes involving soot particles, the following are included in the model: inception, condensation, surface growth and oxidation, and coagulation. Inception, *i.e.* nucleation of a new soot particle, is modelled by dimerisation of coronene – a seven-ring aromatic compound and the largest species represented by the gas-phase chemistry model. Condensation involves adsorption of a coronene molecule on the surface of an existing soot particle. Surface growth and oxidation are modelled using detailed sets of reactions whose rates depend on the attacked functional site and also the neighbouring ones, which can be provided through statistical correlations obtained from Kinetic Monte Carlo (KMC) simulations [52]. The Linear Process Deferment Algorithm (LPDA) [46] is employed to speed up the calculation of surface reactions.

2.2 Model extensions

In order to model the effects of a wall film in this work, the stochastic particle ensemble is divided into two zones: a wall zone and a bulk zone. The particles in the bulk zone undergo the injection process. The particles in the wall zone represent the region near the wall and are involved in the spray impingement and film evaporation processes. The total mass of the wall zone is assumed as a small fraction of the total in-cylinder mass. The initial mass of the wall particles is (much) smaller than that of the bulk particles in order to resolve the film evaporation due to the quite small amount of fuel in the film. Mixing occurs both within and between each zone with different models. A model based on proximity in composition space [67] is used in each of the zones and Curl's model [12] is used for the mixing between zones. Chemical reactions, as in the original model, occur at every time-step in every particle, while the heat transfer to the cylinder wall only occurs in the wall zone.

The wall film is formed due to spray impingement. In terms of the special conditions of the GDI engines during the injection process, such as the 3-20 MPa injection pressure [53], relatively low back pressure, and high piston surface temperature, the spray impingement model should be carefully chosen. While several impingement models have

been proposed in the literature, the model by Bai and Gosman [1, 3] is employed in this study as it has been validated in injection experiments of GDI engines and used in 3D CFD simulations [31, 34, 58]. It should be noted that Su et al. [66] used the same model to simulate spray impingement with SRM. In the current work, this approach is extended to include the presence of a wall film. According to the Bai and Gosman model [1, 3], assuming a wetted wall, the regimes of post-impingement droplets are determined by the Weber number We:

$$\begin{aligned} \text{Stick:} \quad & \mathrm{We} \leqslant 2 \\ \text{Rebound:} \quad & 2 < \mathrm{We} \leqslant 20 \\ \text{Spread:} \quad & 20 < \mathrm{We} \leqslant \mathrm{We_c} \\ \text{Splash:} \quad & \mathrm{We_c} < \mathrm{We} \\ \mathrm{We} =& \frac{\rho_\mathrm{l} d_\mathrm{d} v_\mathrm{in}^2}{\sigma} \\ \mathrm{We_c} =& 1320 \mathrm{La}^{-0.18} \qquad \text{with} \qquad \mathrm{La} = \frac{\rho_\mathrm{l} \sigma d_\mathrm{d}}{\mu^2}, \end{aligned} \tag{1}$$

where ρ_l is the liquid density, d_d is the incident droplet diameter, v_in is the normal component of incident droplet velocity, σ is the droplet surface tension, La is the Laplace number, and μ is the liquid viscosity.

In the rebound regime, none of the impingement droplets will stick to the wall and the reflected droplets have the same size as the impinging ones. In the spread regime, all of the impingement droplets will become part of the film. In the splash regime, some of the incident droplets will be transferred to the wall film, while the remaining ones, called secondary droplets, will be rebounded. The split ratio γ of the droplet mass in the two parts is given by [1]

$$\gamma = \frac{\Delta m_\mathrm{w}}{\Delta m_\mathrm{w} + \Delta m_\mathrm{film}} = 0.2 + 0.9a, \tag{2}$$

where Δm_w and Δm_film are droplet mass rebounded and transferred to wall film, respectively, and a is a random number distributed uniformly between 0 and 1. γ can exceed unity, which accounts for splashing droplets entraining liquid from the wall film.

In order to predict the size of the secondary droplets, the model by Han et al. [21] is employed, which is based on several experimental observations of the droplet impingement. A type of Nukiyama-Tanasawa function is used to model the size distribution of the rebounded droplets. Thus, the Sauter Mean Diameter (SMD) d'_d of the secondary droplet size distribution is given by [1, 3, 21]:

$$\begin{aligned} d'_\mathrm{d} &= 2.16 d_\mathrm{m} \\ d_\mathrm{m} &= \left[\frac{\gamma}{30(\frac{\mathrm{We}}{\mathrm{We_c}} - 1)} \right]^{1/3} d_\mathrm{d}. \end{aligned} \tag{3}$$

Furthermore, mass transfer from the wall film to the wall zone takes place due to evaporation of the wall film. The film evaporation rate $\dot{m}_\mathrm{film}$ is calculated using [2]

$$\dot{m}_\mathrm{film} = \frac{\mathrm{Sh} \rho_\mathrm{g} D (Y_\infty - Y_\mathrm{fs})}{l(1 - Y_\mathrm{fs})}, \tag{4}$$

Table 1: *Physical parameters used in the simulation.*

Parameter	Value	Unit
ρ_l	762.9	kg/m^3
σ	21	mN/m
μ	3.43	mm^2/s
Q_f	0.3	MJ/kg
Re	10667	-
Sc	3.75	-
D	4.0	mm^2/s

where Sh denotes the Sherwood number, ρ_g the density of the surrounding gas, D the fuel/air binary diffusion coefficient, Y_fs the fuel mass fraction at the film surface obtained from the Clausius-Clapeyron equation, and Y_∞ the fuel mass fraction in the surrounding gas far from the surface. The Sherwood number is calculated from the Reynolds number Re and the Schmidt number Sc according to [73]

$$\mathrm{Sh} = 0.332\mathrm{Re}^{1/2}\mathrm{Sc}^{1/3}. \tag{5}$$

l is defined as $l = \frac{l_0}{\delta_0}\delta$, where the ratio of characteristic length l_0 and characteristic film thickness δ_0 is assumed as 100 according to French's experiments [17]. The film thickness δ is determined by Nagaoka's model [41], $\delta = 2\sigma/(\rho_\mathrm{l} v_\mathrm{in}^2)$. The temperature of the film is assumed constant and equal to the temperature of the cylinder wall, so the heat transfer between the film and the cylinder wall as well as evaporative cooling of the film are ignored.

Table 1 shows the values used for the physical parameters appearing above.

3 Algorithm

3.1 Spray, impingement, and wall film evaporation process

The cylinder is divided into two zones, the bulk zone, which is denoted by a subscript "b", and the wall zone, which is denoted by a subscript "w". The model extensions described in the previous section are implemented as follows:

1. In each time-step, calculate the spray penetration $S(t)$ according to [22]

$$S(t) = \begin{cases} 0.39(\frac{2\Delta p}{\rho_\mathrm{l}})^{1/2}t, & t < t_\mathrm{break} \\ 2.95(\frac{\Delta p}{\rho_\mathrm{g}})^{1/4}(d_0 t)^{1/2} & t > t_\mathrm{break} \end{cases} \tag{6}$$

$$t_\mathrm{break} = \frac{28.65\rho_\mathrm{l} d_0}{(\rho_\mathrm{g}\Delta p)^{1/2}}, \tag{7}$$

where t is the time since start of injection, Δp is the pressure drop across the nozzle, d_0 is

the nozzle diameter, ρ_l and ρ_g are the fuel liquid and gas densities respectively, and t_break is the spray break-up time.

Calculate the current spray penetration volume

$$V_\mathrm{pen} = \frac{\pi}{3}\sin^2\left(\frac{\theta}{2}\right)S(t)^3, \tag{8}$$

where θ is the cone angle of the spray.

2. Pick stochastic particles to be penetrated by the spray as follows: Let U denote the set of indices of all particles which have been chosen since the start of injection. Then, add new particles to this set, picked uniformly randomly from the bulk zone, until their total volume

$$V_\mathrm{par} = \sum_i V^{(i)} \qquad \forall i \in U \tag{9}$$

at least equals the penetration volume, *i.e.* $V_\mathrm{par} \geqslant V_\mathrm{pen}$. This ensures that a set of particles is chosen such that their combined volume approximates Eqn. 8.

3. Assign to each of the chosen particles a value of $m_\mathrm{liq}^{(i)}$ proportional to the statistical weight $W^{(i)}$, *i.e.* the particle mass, such that the total injected mass $\sum m_\mathrm{liq}^{(i)}$ during the time-step Δt equals $\dot{m}_\mathrm{fuel}\Delta t$, where $\dot{m}_\mathrm{fuel}$ is the injected mass flow rate and $m_\mathrm{liq}^{(i)}$ is the mass of liquid fuel in the i^th particle:

$$m_\mathrm{liq}^{(i)} = \frac{W^{(i)}}{\sum_j W^{(j)}}\dot{m}_\mathrm{fuel}\Delta t. \tag{10}$$

In each of the chosen particles, initialise the droplet diameter $d_\mathrm{d}^{(i)} = d_\mathrm{n}$, where d_n is an initial diameter defined by the user according to injection data and calculate the droplet numbers according to

$$N_\mathrm{d}^{(i)} = \frac{6m_\mathrm{liq}^{(i)}}{\pi\rho_\mathrm{l}d_\mathrm{d}^{(i)3}} \qquad \forall i \in 1,\ldots,N_{par}. \tag{11}$$

4. If

$$S(t)\sin\left(\frac{\theta}{2}\right) > \frac{\mathrm{Bore}}{2} \qquad \text{or} \qquad S(t)\cos\left(\frac{\theta}{2}\right) > \frac{4V(t)}{\pi\mathrm{Bore}^2}, \tag{12}$$

where $V(t)$ is the current cylinder volume, spray impingement occurs, go to step 5. Otherwise, go to step 6.

5. The particles involved in the impingement are the ones at the tip of the spray, *i.e.* the ones newly selected in the current time-step. In each of these particles, determine the regimes of the post-impingement droplets according to Eqn. 1 by calculating the Weber number

$$\mathrm{We} = \frac{\rho_\mathrm{l}d_\mathrm{d}\left[v(t)\cos\left(\frac{\theta}{2}\right)\right]^2}{\sigma}, \tag{13}$$

where $v(t) = \mathrm{d}S(t)/\mathrm{d}t$ denotes the velocity of the tip of the spray. If a particle contains droplets of a diameter such that the Weber number corresponds to the spread regime, the fuel droplet mass involved in the impingement is added to the wall film mass and then the droplet mass and number, particle mass, and enthalpy of each particle in the bulk zone are updated.

If the particle locates in the rebound regime, all of the fuel involved in the impingement is transferred to the wall zone Δm_{w} and these droplets have the same size as the impinging droplets, *i.e.* $d_{\mathrm{d}}^{\prime(i)} = d_{\mathrm{d}}^{(i)}$. The droplet size of the updated particles in the wall zone is given by

$$d_{\mathrm{dw}}^{(i)} = \left[\frac{6(m_{\mathrm{lw}}^{(i)} + \Delta m_{\mathrm{lw}}^{(i)})}{\pi\rho_{\mathrm{l}}(N_{\mathrm{dw}}^{(i)} + \Delta N_{\mathrm{dw}}^{(i)})}\right]^{1/3}, \tag{14}$$

where $\Delta m_{\mathrm{lw}}^{(i)}$ and $\Delta N_{\mathrm{dw}}^{(i)}$ are the mass and number of droplets added to each particle, which are determined through equations similar to Eqns. 10 and 11, respectively.

If the particle locates in the splash regime, the mass of the impinging droplets is distributed to the wall film mass and droplet mass in the particles in the wall zone (similar to Eqn. 10) according to the split ratio γ, which is calculated by Eqn. 2. The rebounded droplet size $d_{\mathrm{d}}^{\prime(i)}$ is calculated by Eqn. 3.

6. Calculate the film evaporation rate $\dot{m}_{\mathrm{film}}$ according to Eqn. 4, with the average fuel mass fraction in the wall zone taken as Y_{∞}. Update the composition and temperature of the particles in the wall zone as follows: Add to the mass of each particle in the wall zone a value of $\Delta m_{\mathrm{fuel}}^{(i)}$ proportional to the statistical weight to represent the evaporated mass, *i.e.*

$$\Delta m_{\mathrm{fuel}}^{(i)} = \frac{W^{(i)}}{\sum_j W^{(j)}}\dot{m}_{\mathrm{film}}\Delta t \qquad \forall\text{particles } i \text{ in the wall zone.} \tag{15}$$

Update the enthalpy according to $\left[W^{(i)}H^{(i)} + \Delta m_{\mathrm{fuel}}^{(i)}(H_{\mathrm{f}}^{(i)} - Q_{\mathrm{f}})\right]/\left(W^{(i)} + \Delta m_{\mathrm{fuel}}^{(i)}\right)$, and the statistical weight $W^{(i)}$ for all particles in the wall zone, where $H^{(i)}$ is the enthalpy in the last time-step, Q_{f} is the vaporization heat, and $H_{\mathrm{f}}^{(i)}$ is the fuel enthalpy of the film. Update the particle masses and gas-phase species mass fractions according to mass conservation.

7. Update the liquid fuel mass, statistical weight, gas-phase species mass fractions, and enthalpy of all particles in both bulk and wall zones after the droplet evaporation, which is treated as in previous work [35].

3.2 The mixing process between the wall zone and bulk zone

The characteristic rate for the exchange of mass between the wall and bulk zones is defined as

$$\beta = \frac{\text{Exchange mass flow rate}}{M_{\mathrm{tot,w}}}, \tag{16}$$

where $M_{\mathrm{tot,w}}$ denotes total mass in the wall zone. Thus, in a time-step Δt, the mass exchanged between the zones is given by $\beta M_{\mathrm{tot,w}}\Delta t$. Larger β corresponds to more rapid mixing.

The mass exchange process is implemented as follows:

1. Pick particles uniformly randomly from the wall zone until the combined mass of these particles exceeds the exchange mass, *i.e.* $\sum_j W^{(j)} \geqslant \beta M_{\mathrm{tot,w}}\Delta t$, where the sum is understood to range over the chosen particles only.

2. The exchange mass for each of the chosen particles $\Delta m_{\mathrm{w}}^{(i)}$ is proportional to the statistical weight and calculated by

$$\Delta m_{\mathrm{w}}^{(i)} = \frac{W^{(i)}}{\sum_j W^{(j)}} \beta M_{\mathrm{tot,w}}\Delta t. \tag{17}$$

3. Perform a procedure analogous to steps 1 and 2 for the bulk zone to obtain the particles involved in the mixing process and the exchange mass for each of the chosen particles $\Delta m_{\mathrm{b}}^{(i)}$.

4. Update all particles in the wall zone by averaging the information in the chosen particles in the bulk zone. The statistical weight of each particle does not change. The gas-phase species mass fractions $Y_j^{(i)}$ of the i^{th} wall particle are updated according to

$$Y_j^{(i)} \leftarrow \Big(1 - \frac{\Delta m_{\mathrm{w}}^{(i)}}{W^{(i)}}\Big) Y_j^{(i)} + \frac{\Delta m_{\mathrm{w}}^{(i)}}{W^{(i)}} \Big(\frac{1}{\sum_k W^{(k)}} \sum_k Y_j^{(k)} W^{(k)} \Big), \tag{18}$$

where the sums over k are understood to range over the chosen bulk particles only. The liquid mass $m_{\mathrm{liq}}^{(i)}$ and droplet number $N_{\mathrm{d}}^{(i)}$ are updated in a similar fashion. The droplet diameter is then recalculated as

$$d_{\mathrm{d}}^{(i)} = \Big(\frac{6 m_{\mathrm{liq}}^{(i)}}{\pi \rho_{\mathrm{l}} N_{\mathrm{d}}^{(i)}} \Big)^{1/3}. \tag{19}$$

5. Update the enthalpy for all particles in the wall zone according to $\big[(W^{(i)} - \Delta m_{\mathrm{w}}^{(i)}) H_{\mathrm{w}}^{(i)} + \Delta m_{\mathrm{w}}^{(i)} H_{\mathrm{b}}^{(i)}\big] / W^{(i)}$, where $H_{\mathrm{w}}^{(i)}$ and $H_{\mathrm{b}}^{(i)}$ are the enthalpy of particles in the wall zone and the bulk zone before the mixing, respectively.

6. Similar to step 4 and 5, update the chosen particles in the bulk zone.

4 Experimental setup and results

The engine used in this study is a Geely four-cylinder GDI engine. Engine specifications are shown in **Table 2**. The test fuel is commercial gasoline, with a Research Octane Number (RON) of 93. The ETAS INCA electronic control system can flexibly control the injection timing and duration. Engine-out particles are sampled from the exhaust manifold

Table 2: *Test engine specifications.*

Engine type	4-cylinder turbo-charged GDI engine
Bore × Stroke	75 mm × 73.5 mm
Displacement	1.3 L
Compression ratio	10.2
Injector	6 holes
Injector cone angle	72 deg
Intake valve open	389 CAD BTDC
Intake valve close	167 CAD BTDC
Exhaust valve open	172 CAD ATDC
Exhaust valve close	382 CAD ATDC

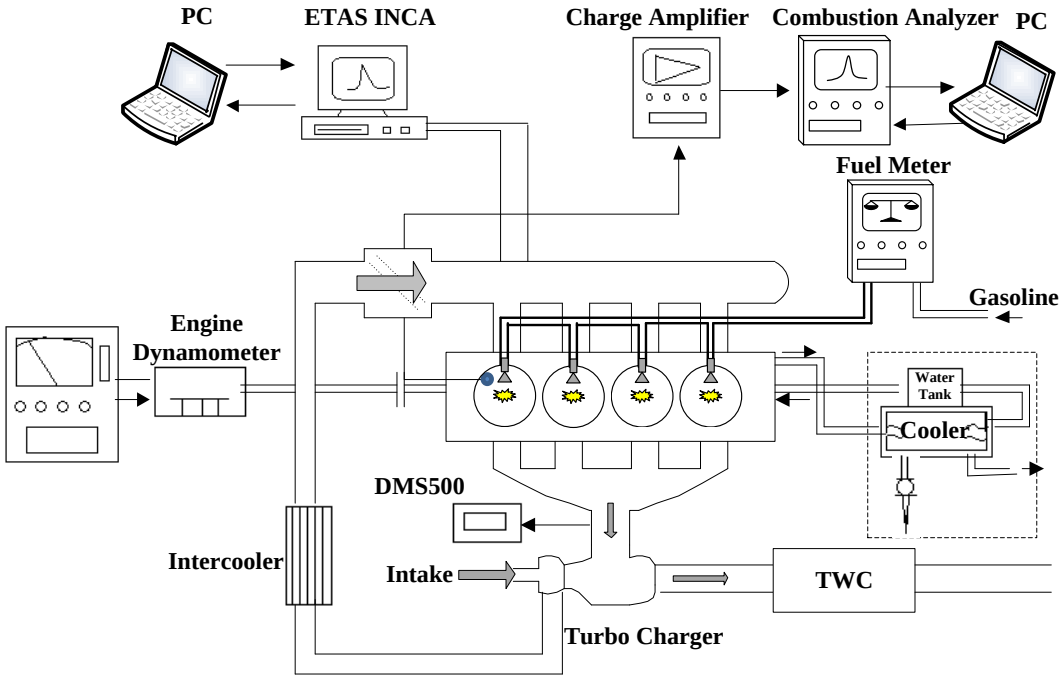

Figure 1: *Engine system schematic.*

and analysed by a Cambustion DMS500 differential mobility spectrometer to obtain the particle size distribution. A schematic of the experimental apparatus is shown in **Fig. 1**.

In the test, the engine speed is 2000 rpm at a torque of 137 Nm. The air-fuel ratio is controlled at the stoichiometric ratio and the spark timing is 3 CAD ATDC. The intake temperature and pressure are 313 K and 0.156 MPa, respectively. Single injection is used with 13 MPa injection pressure. In the experiments, different injection timings varying from 120 CAD BTDC to 330 CAD BTDC are compared, which cover large parts of the intake and compression stroke. It can be seen in **Fig. 2** that when the injection is too early (330 CAD BTDC), particulate emissions increase significantly, especially of particles with size larger than 30 nm, which mainly consist of soot [26]. Similar results

can be found in [15, 50]. At 330 CAD BTDC, the distance between the injector and the piston is too short to avoid the spray impinging. It should be noted that the injector, producing sprays with a relatively small cone angle, is designed for injections near bottom dead centre. The time for spray vaporisation and mixing is sufficiently long that the possibility of soot formation from locally rich conditions occurring in the bulk mixture can be excluded. Thus, it is suggested that the wall film is the only source of these large particles due to the late evaporation of the film and then the formation of locally rich regions near the piston wall. No systematic variation in the particle size distribution can be observed for a wide range of injection timings. It is concluded from this that the mechanism of formation for these particles is likely to be unrelated to spray impingement on the piston.

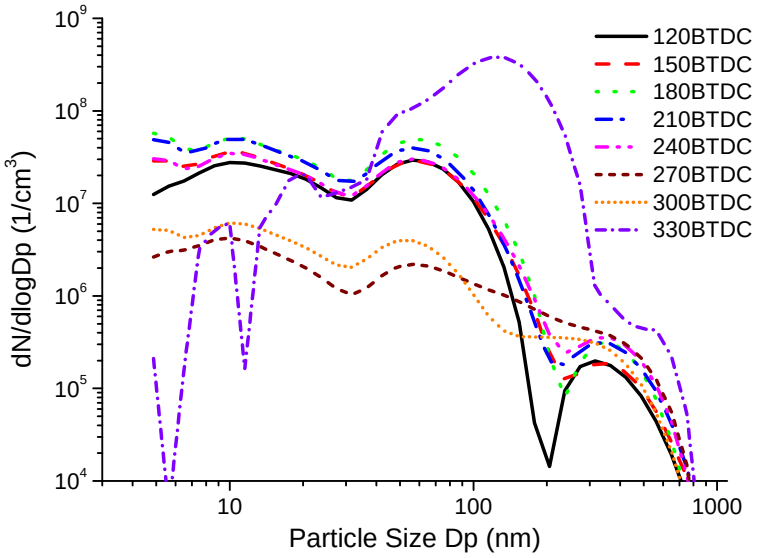

Figure 2: *Engine-out particle size distributions for different injection timings as measured by DMS500.*

5 Simulation results and discussion

5.1 Parameter sweeps

Two important parameters are introduced in the modified mixing model, the turbulent mixing rate in the wall zone and the fraction β which determines the mixing between the wall zone and the bulk zone. It is necessary to discuss the influence of the two parameters. **Figure 3** shows the effect of β on the average temperature and the equivalence ratio in the bulk and wall zone, respectively. A large β means the wall and bulk zones mix strongly, so the average temperature is similar for the two zones and the equivalence ratio rapidly approaches the same value in both zones after the wall film is completely evaporated. By decreasing β, the bulk zone temperature is slightly influenced, but the wall zone temperature drops significantly. Also, the wall zone becomes rich with small β. Since, experimentally, low temperatures and fuel-rich mixtures are found near the wall during

combustion [64], it is assumed that a small β is more realistic, *i.e.* the mass and heat exchange between the wall and the bulk zones is assumed to be slow.

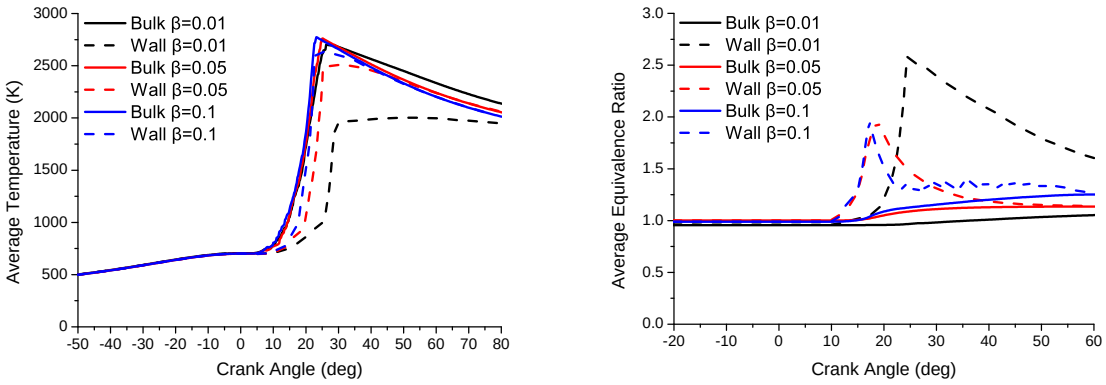

(a) *Temperature.* **(b)** *Equivalence ratio.*

Figure 3: *The average temperature and equivalence ratio of the wall and bulk particles with different β.*

Figure 4 shows the temperature and equivalence ratio in the bulk and wall zone with different mixing rate in the wall zone. As a result of the heat transfer with the wall and the early flame propagation in the bulk zone, the temperature in the wall zone is lower than in the bulk zone, which slows the mixing process near the wall. Thus, a lower mixing rate for the wall zone is used in the study. In order to describe the relation of the turbulence intensities in the wall and the bulk zone, a parameter κ is defined as

$$\kappa = \frac{\tau_{\text{bulk}}}{\tau_{\text{wall}}}, \tag{20}$$

where τ_{bulk} and τ_{wall} are the mixing time in the wall and bulk zone, respectively. It should be noted that for SI simulation, the particle ensemble is divided into three zones: unburned, entrained and burned [14], and these zones are independent of the bulk/wall partitioning. That is, any bulk or wall particle can be part of any of the three SI zones. The mixing time τ_{bulk} and τ_{wall} can vary in different SI zones, but κ is the same for these zones (κ_{unburned}=$\kappa_{\text{entrained}}$=$\kappa_{\text{burned}}$). For the results shown in **Fig. 4**, the mixing rate in the bulk zone is kept the same and κ is set at 0.01, 0.1, and 0.5, respectively. Unsurprisingly, the bulk zone is barely affected by the mixing rate in the wall zone, while the slow mixing provides lower temperature and richer mixture in the wall zone. Ratios below 0.1 do not significantly affect the temperature and the equivalence ratio in the wall zone.

5.2 Wall film soot simulation

As mentioned in section 4, the experimental case with the earliest injection timing (330 CAD BTDC) is the only one which exhibits a significant increase in particle emissions above the baseline. For this reason, this case is chosen to be simulated. The measured particle size for comparison is modified as the difference between the results in the 330 CAD BTDC case and the 300 CAD BTDC case. The time-step is 0.2 CAD and 100 SRM

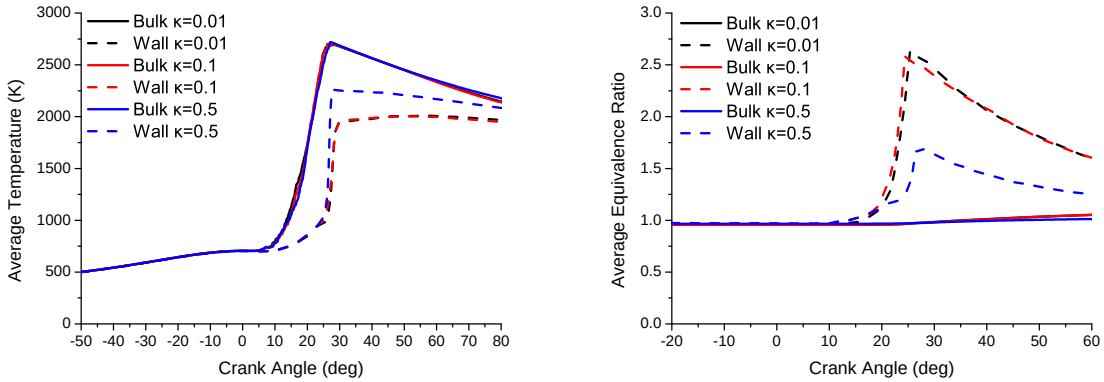

(a) *Temperature.* **(b)** *Equivalence ratio.*

Figure 4: *The average temperature and equivalence ratio of the wall and bulk particles with different κ. The rise in equivalence ratio is due to the wall film evaporation, which itself increases due to the temperature rise as a consequence of combustion heat release.*

particles are used. The calculation duration is from the intake valve open to the exhaust valve open. A breathing model is used to simulate the intake process [14]. 93 mass% *iso*-octane and 7 mass% *n*-heptane are used to match the RON of the test fuel. Model parameters such as the turbulent mixing time and the parameters in the flame propagation model are calibrated to match the cylinder pressure and heat release rate with the experimental data. These parameters are listed in **Table 3**. **Figure 5** shows a comparison of in-cylinder pressure and heat release rate between experiment and simulation.

Table 3: *Key model parameters used in the simulation.*

Parameter	Value	Unit
Initial mass ratio of wall/bulk zone	0.01	-
Particle number in wall zone	50	-
Particle number in bulk zone	50	-
Mixing time in bulk burnt zone	2.5	ms
Mixing time in bulk entrained zone	0.25	ms
β	0.01	1/s
κ	0.1	-

Figure 6 shows the time-evolution of the liquid fuel mass in the wall film. The liquid film contains about 5.4 mg of fuel at spark timing (3 CAD ATDC), which is about 15% of the total injected fuel. Subsequently, the film evaporates rapidly, which can be attributed to the rising temperature in the wall zone. The average temperature and equivalence ratio of the wall and bulk particles as a function of crank angle, respectively, are shown by the corresponding curves ($\kappa = 0.1$) in Fig. 4. The average temperature of the wall particles is lower than that of the bulk particles after the start of ignition (about 6 CAD ATDC). After 10 CAD ATDC, the evaporation rate of wall film increases (**Fig. 6**), which leads

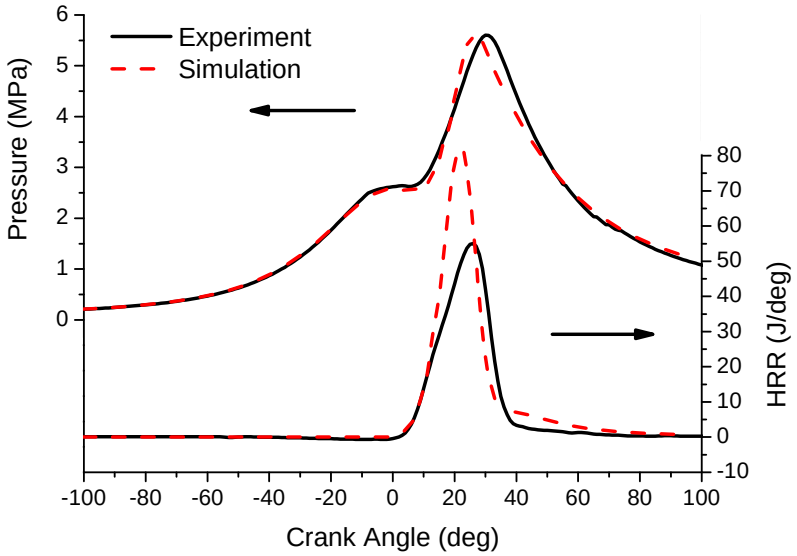

Figure 5: *The cylinder pressure and heat release rate in the experiment and simulation.*

to an increase of the equivalence ratio in the wall particles. Attributed to the mixing between the wall zone and the bulk zone, the temperature of the bulk particles drops and the equivalence ratio of the bulk particles slightly increases.

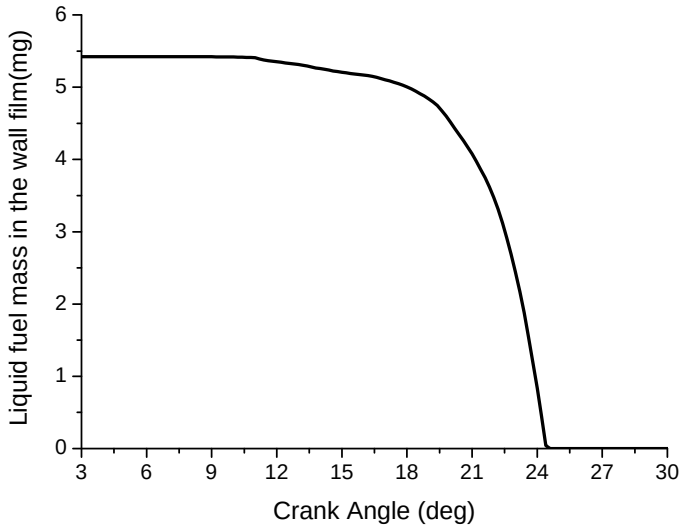

Figure 6: *Simulated time-evolution of the liquid fuel mass in the wall film.*

In order to trace the time-evolution of equivalence ratio and temperature of each particle, Φ-T distributions are plotted at several crank angles in **Fig.** 7. In the figure, the blue dots represent the wall particles and the red ones the bulk particles. At 6 CAD ATDC, all of the particles are unburnt and the equivalence ratio is close to 1. At 10 CAD ATDC, the bulk particles firstly burn at the stoichiometric condition. Then the temperature of the wall particles increases, which can be attributed to ignition and mixing with the bulk particles. At the same time, the mixture becomes richer due to the film evaporation and enters the soot peninsula (from 22 CAD ATDC). These rich mixtures in the wall zone

become the source of the soot formation. After the soot formation, the low temperature of the wall particles (< 1600 K) decreases the oxidation rate leading to the final engine-out soot emissions, which is consistent with the optical results by Stojkovic et al. [64].

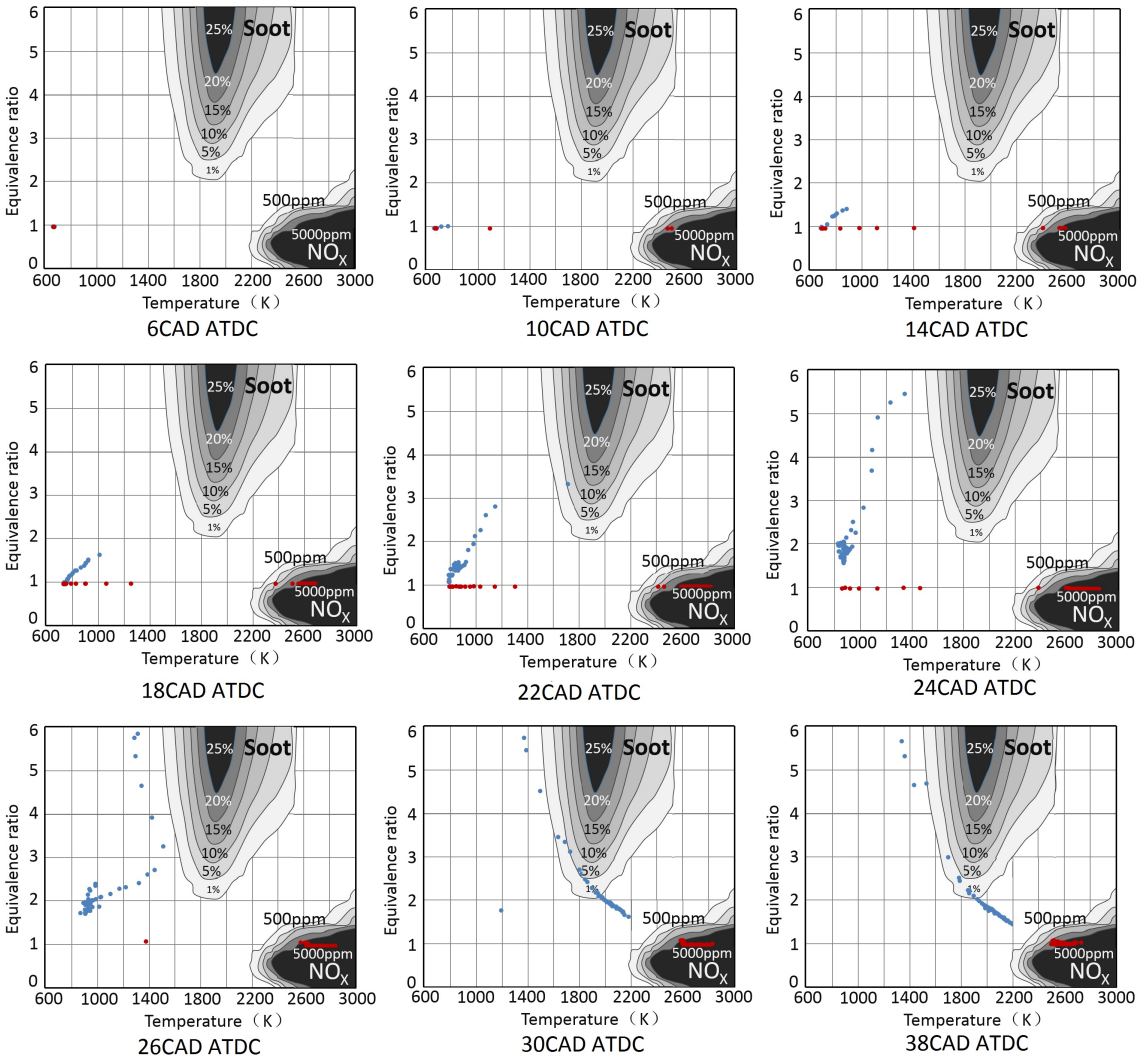

Figure 7: *Equivalence ratio-temperature diagram of the wall and bulk particles at different crank angles in the simulation. The blue dots represent the wall particles and the red ones represent the bulk particles. The soot and NO_x iso-lines are adopted from Kamimoto and Bae [24].*

All of the rates of the processes in the particulate phase are displayed in **Fig. 8** as a function of crank angle. In **Fig. 8a**, the coronene inception, condensation and coagulation rates are shown. The inception rate peaks around 50 CAD ATDC. **Figure 8b** shows the growth rate via acetylene addition and free-edge desorption. The acetylene free-edge growth is the main growth process at the early stage, while the free-edge desorption is more important at the late stage. Among a number of the five-member ring process, the desorption process has the highest rate, as shown in **Fig. 8c**. Soot oxidation by OH dominates the oxidation process, as depicted in **Fig. 8d**.

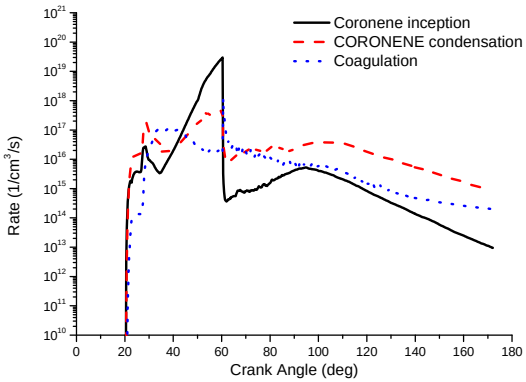

(a) *Inception, condensation, and coagulation processes.*

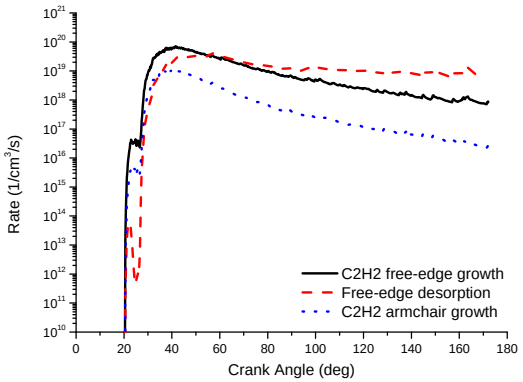

(b) *Edge growth and desorption processes.*

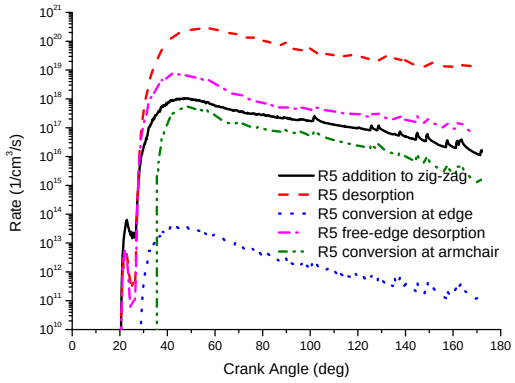

(c) *Five-member ring processes.*

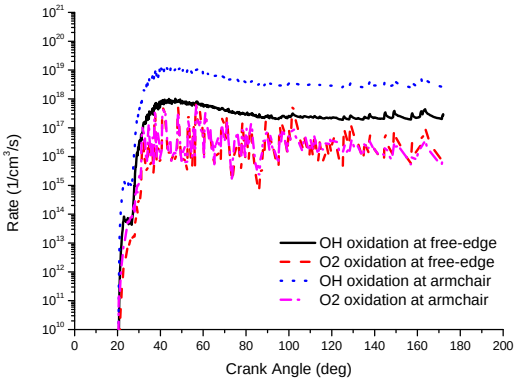

(d) *Oxidation processes.*

Figure 8: *The rates of the processes in the particulate phase.*

Figure 9a shows the experimental as well as simulated particle size distributions. The simulated number densities at exhaust valve open (172 CAD ATDC) are of the same order of magnitude as the experimental data. The number of particles with small size is over-predicted in the simulation, which may be explained by particle oxidation and coagulation in the exhaust and sample system in the experiment. The size of the particles in the main mode of the experimental distribution is under-predicted by about a factor of two. This, however, is sensitive to the detailed equivalence ratio-temperature history of the fluid parcels in which most of the soot is formed, and to the surface growth and oxidation rate constants in the soot model.

The particle size distribution at different crank angles in the simulation is displayed in **Fig.** 9b. The small particles (< 10 nm) form when the inception rate is high and then the number of the large particles (> 100 nm) increases as a consequence of growth and coagulation. At a later stage of the cycle, a decrease in the particle number is found after the main heat release process due to oxidation.

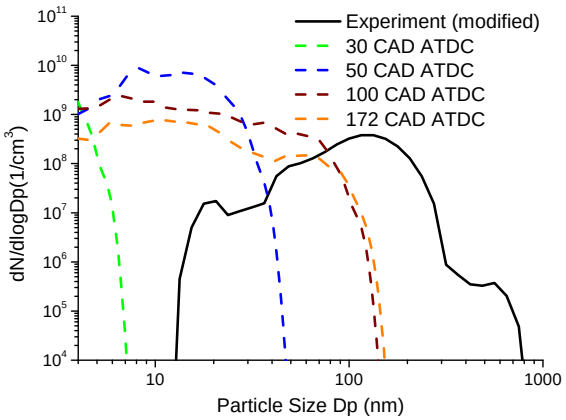

(a) *Comparison of the particle size distribution in the experiment and simulation.*

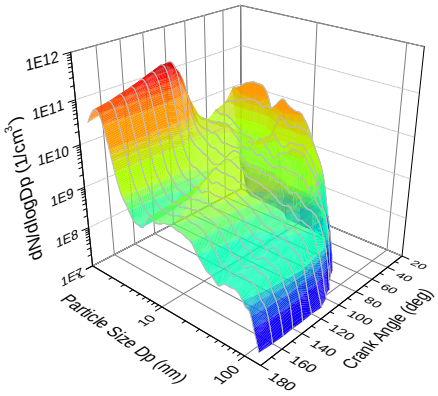

(b) *Time-evolution of the particle size distribution in the simulation.*

Figure 9: *Soot particle size distributions.*

6 Conclusions

Coupling a spray impingement model and wall film evaporation model, a PDF-based Stochastic Reactor Model is extended to simulate the combustion process in a GDI engine. By dividing the cylinder into a wall and bulk zone, the spray impingement process and the distribution of equivalence ratio and temperature near the wall can be described. The combustion chamber wall is assumed to exchange heat directly only with the wall zone. The mixing inside the zones and between the two zones is calculated by different turbulent mixing models. A detailed population balance soot model, which can capture soot morphology and chemical composition, is incorporated to simulate the soot formation by the wall film evaporation.

The effect of key parameters on temperature and equivalence ratio is investigated. The mixing rate between the wall and bulk zone has a significant effect on the temperature and equivalence ratio in the wall zone. A small mixing rate decreases the wall zone temperature and increases the equivalence ratio, compared to well-mixed conditions. The mixing rate in the wall zone only has a minor effect if the rate is less than one tenth of the mixing rate in the bulk zone.

A four-cylinder GDI engine is operated stoichiometrically at 2000 rpm and 137 Nm torque. The effect of spray impingement on the soot formation is tested by sweeping the injection timing from 120 CAD BTDC to 330 CAD ATDC. The earliest injection (330 CAD ATDC) produces significantly higher particle emissions and this case is simulated by the current model. The in-cylinder pressure and heat release rate in the simulation show satisfactory agreement with the experimental data. It is found that after the ignition, the wall zone has lower temperature and higher equivalence ratio than the bulk zone as a consequence of localised heat exchange with the cylinder wall, slow mixing with the bulk charge, and the wall film evaporation. By tracing the particles in an equivalence ratio-temperature diagram, it is demonstrated that the rich mixture near the wall becomes a source of soot formation. The particle size distribution in the simulation has the same

order of magnitude as the experimental one.

Acknowledgements

The authors would like to acknowledge the National Key Basic Research Plan (Chinese ”973” Plan) under Grant No. 2013CB228502. This project was partly funded by the National Research Foundation (NRF), Prime Minister’s Office, Singapore under its Campus for Research Excellence and Technological Enterprise (CREATE) programme. The authors are grateful to CMCL innovations for technical support related to the SRM Engine Suite software through their global academic partnership programme, and to Dr Radomir I. Slavchov for valuable discussions and comments.

References

[1] C. Bai and A. Gosman. Development of methodology for spray impingement simulation. *SAE Technical Paper 950283*, 1995. doi:10.4271/950283.

[2] C. Bai and A. Gosman. Mathematical modelling of wall films formed by impinging sprays. *SAE Technical Paper 960626*, 1996. doi:10.4271/960626.

[3] C. Bai, H. Rusche, and A. Gosman. Modeling of gasoline spray impingement. *Atomization and Sprays*, 12(1-3):1–27, 2002. doi:10.1615/AtomizSpr.v12.i123.10.

[4] M. Balthasar and M. Kraft. A stochastic approach to calculate the particle size distribution function of soot particles in laminar premixed flames. *Combustion and Flame*, 133(3):289–298, 2003. doi:10.1016/S0010-2180(03)00003-8.

[5] A. Berndorfer, S. Breuer, W. Piock, and P. V. Bacho. Diffusion combustion phenomena in GDi engines caused by injection process. *SAE Technical Paper 2013-01-0261*, 2013. doi:10.4271/2013-01-0261.

[6] A. Bhave, M. Kraft, L. Montorsi, and F. Mauss. Sources of CO emissions in an HCCI engine: A numerical analysis. *Combustion and Flame*, 144(3):634–637, 2006. doi:10.1016/j.combustflame.2005.10.015.

[7] M. Braisher, R. Stone, and P. Price. Particle number emissions from a range of European vehicles. *SAE Technical Paper 2010-01-0786*, 2010. doi:10.4271/2010-01-0786.

[8] F. Catapano, S. D. Iorio, M. Lazzaro, P. Sementa, and B. M. Vaglieco. Characterization of ethanol blends combustion processes and soot formation in a GDI optical engine. *SAE Technical Paper 2013-01-1316*, 2013. doi:10.4271/2013-01-1316.

[9] M. Celnik, R. Patterson, M. Kraft, and W. Wagner. Coupling a stochastic soot population balance to gas-phase chemistry using operator splitting. *Combustion and Flame*, 148(3):158–176, 2007. doi:10.1016/j.combustflame.2006.10.007.

[10] M. Celnik, A. Raj, R. West, R. Patterson, and M. Kraft. Aromatic site description of soot particles. *Combustion and Flame*, 155(1-2):161–180, 2008. doi:10.1016/j.combustflame.2008.04.011.

[11] cmcl innovations. srm engine suite, version 8.2, 2015. http://www.cmclinnovations.com/srm-suite/.

[12] R. Curl. Dispersed phase mixing: I. Theory and effects in simple reactors. *AIChE Journal*, 9(2):175–181, 1963. doi:10.1002/aic.690090207.

[13] J. Etheridge, S. Mosbach, M. Kraft, H. Wu, and N. Collings. Modelling soot formation in a DISI engine. *Proceedings of the Combustion Institute*, 33(2):3159–3167, 2011. doi:10.1016/j.proci.2010.07.039.

[14] J. Etheridge, S. Mosbach, M. Kraft, H. Wu, and N. Collings. Modelling cycle to cycle variations in an SI engine with detailed chemical kinetics. *Combustion and Flame*, 158(1):179–188, 2011. doi:10.1016/j.combustflame.2010.08.006.

[15] C. Farron, N. Matthias, D. Foster, M. Andrie, R. Krieger, P. Najt, K. Narayanaswamy, A. Solomon, and A. Zelenyuk. Particulate characteristics for varying engine operation in a gasoline spark ignited, direct injection engine. *SAE Technical Paper 2011-01-1220*, 2011. doi:10.4271/2011-01-1220.

[16] M. Fatouraie, M. Wooldridge, and S. Wooldridge. In-cylinder particulate matter and spray imaging of ethanol/gasoline blends in a direct injection spark ignition engine. *SAE International Journal of Fuels and Lubricants*, 6(1):1–10, 2013. doi:10.4271/2013-01-0259.

[17] W. French, D. Rose, P. Kelly-Zion, and C. Prusell. Analysis of evaporating fuel films using shadowgraph and schlieren imaging techniques. *SAE Technical Paper 2008-01-2443*, 2008. doi:10.4271/2008-01-2443.

[18] M. Goodson and M. Kraft. An efficient stochastic algorithm for simulating nanoparticle dynamics. *Journal of Computational Physics*, 183(1):210–232, 2002. doi:10.1006/jcph.2002.7192.

[19] B. Graskow, D. Kittelson, M. Ahmadi, and J. Morris. Exhaust particulate emissions from a direct injection spark ignition engine. *SAE Technical Paper 1999-01-1145*, 1999. doi:10.4271/1999-01-1145.

[20] P. Guthrie. A review of fuel, intake and combustion system deposits issues relevant to 4-stroke gasoline direct fuel injection engines. *SAE Technical Paper 2001-01-1202*, 2001. doi:10.4271/2001-01-1202.

[21] Z. Han, Z. Xu, and N. Trigui. Spray/wall interaction models for multidimensional engine simulation. *International Journal of Engine Research*, 1(1):127–146, 2000. doi:10.1243/1468087001545308.

[22] H. Hiroyasu, T. Kadota, and M. Arai. Development and use of a spray combustion modeling to predict diesel engine efficiency and pollutant emissions (part 1 combustion modeling). *Bulletin of the JSME*, 26(214):569–575, 1983. doi:10.1299/jsme1958.26.569.

[23] Q. Jiao and R. Reitz. Modeling of equivalence ratio effects on particulate formation in a spark-ignition engine under premixed conditions. *SAE Technical Paper 2014-01-1607*, 2014. doi:10.4271/2014-01-1607.

[24] T. Kamimoto and M. Bae. High combustion temperature for the reduction of particulate in diesel engines. *SAE Technical Paper 880423*, 1988. doi:10.4271/880423.

[25] M. Kim, H. Cho, Y. Cho, and K. Min. Computational and optical investigation of liquid fuel film on the cylinder wall of an SI engine. *SAE Technical Paper 2003-01-1113*, 2003. doi:10.4271/2003-01-1113.

[26] D. Kittelson. Engines and nanoparticles: a review. *Journal of Aerosol Science*, 29 (5-6):575–588, 1998. doi:10.1016/S0021-8502(97)10037-4.

[27] M. Kraft, P. Maigaard, F. Mauss, M. Christensen, and B. Johansson. Investigation of combustion emissions in a homogeneous charge compression injection engine: measurements and a new computational model. *Proceedings of the Combustion Institute*, 28(1):1195–1201, 2000. doi:10.1016/S0082-0784(00)80330-6.

[28] S. Lee and H. Ryou. Modeling of diesel spray impingement on a flat wall. *KSME International Journal*, 14(7):796–806, 2000.

[29] S. Lee and H. Ryou. Development of a new spray/wall interaction model. *International Journal of Multiphase Flow*, 26(7):1209–1234, 2000. doi:10.1016/S0301-9322(99)00080-4.

[30] R. Lindgren and I. Denbratt. Modelling gasoline spray-wall interaction – a review of current models. *SAE Technical Paper 2000-01-2808*, 2000. doi:10.4271/2000-01-2808.

[31] T. Lucchini, G. D'Errico, A. Onorati, G. Bonandrini, L. Venturoli, and R. D. Gioia. Development of a CFD approach to model fuel-air mixing in gasoline direct-injection engines. *SAE Technical Paper 2012-01-0146*, 2012. doi:10.4271/2012-01-0146.

[32] E. Magaril and R. Magaril. *Motor fuels*. KDU, Moscow, 2008.

[33] E. Magaril, R. Magaril, and V. Bamburov. Specific features of combustion in gasoline-driven internal combustion engines. *Combustion, Explosion, and Shock Waves*, 50(1):75–79, 2014. doi:10.1134/S0010508214010092.

[34] A. Montanaro, S. Malaguti, and S. Alfuso. Wall impingement process of a multi-hole GDI spray: Experimental and numerical investigation. *SAE Technical Paper 2012-01-1266*, 2012. doi:10.4271/2012-01-1266.

[35] S. Mosbach, H. Su, M. Kraft, A. Bhave, F. Mauss, Z. Wang, and J. Wang. Dual injection HCCI engine simulation using a stochastic reactor model. *International Journal of Engine Research*, 8(1):41–50, 2007. doi:10.1243/14680874JER01806.

[36] S. Mosbach, A. Aldawood, and M. Kraft. Real-time evaluation of a detailed chemistry HCCI engine model using a tabulation technique. *Combustion Science and Technology*, 180(7):1263–1277, 2008. doi:10.1080/00102200802049414.

[37] S. Mosbach, M. Celnik, A. Raj, M. Kraft, H. Zhang, S. Kubo, and K. Kim. Towards a detailed soot model for internal combustion engines. *Combustion and Flame*, 156 (6):1156–1165, 2009. doi:10.1016/j.combustflame.2009.01.003.

[38] C. Mundo, M. Sommerfeld, and C. Tropea. Droplet-wall collisions: experimental studies of the deformation and breakup process. *International Journal of Multiphase Flow*, 21(2):151–173, 1995. doi:10.1016/0301-9322(94)00069-V.

[39] C. Mundo, C. Tropea, and M. Sommerfeld. Numerical and experimental investigation of spray characteristics in the vicinity of a rigid wall. *Experimental Thermal and Fluid Science*, 15(3):228–237, 1997. doi:10.1016/S0894-1777(97)00015-0.

[40] J. Naber and R. Reitz. Modeling engine spray/wall impingement. *SAE Technical Paper 880107*, 1988. doi:10.4271/880107.

[41] M. Nagaoka, H. Kawazoe, and N. Nomura. Modeling fuel spray impingement on a hot wall for gasoline engines. *SAE Technical Paper 940525*, 1994. doi:10.4271/940525.

[42] C. Naik, L. Liang, K. Puduppakkam, and E. Meeks. Simulation and analysis of in-cylinder soot formation in a gasoline direct-injection engine using a detailed reaction mechanism. *SAE Technical Paper 2014-01-1135*, 2014. doi:10.4271/2014-01-1135.

[43] L. Ntziachristos, A. Mamakos, Z. Samaras, R. Stradling, U. Mathis, M. Mohr, L. Forti, N. Thompson, and C. de Serves. Overview of the European "Particulates" project on the characterization of exhaust particulate emissions from road vehicles: Results for light-duty vehicles. *SAE Technical Paper 2004-01-1985*, 2004. doi:10.4271/2004-01-1985.

[44] P. O'Rourke and A. Amsden. A spray/wall interaction submodel for the KIVA-3 wall film model. *SAE Technical Paper 2000-01-0271*, 2000. doi:10.4271/2000-01-0271.

[45] R. Ortmann, S. Arndt, J. Raimann, R. Grzeszik, and G. Würfel. Methods and analysis of fuel injection, mixture preparation and charge stratification in different direct injected si engines. *SAE Technical Paper 2001-01-0970*, 2001. doi:10.4271/2001-01-0970.

[46] R. Patterson, J. Singh, M. Balthasar, M. Kraft, and J. Norris. The linear process deferment algorithm: a new technique for solving population balance equations. *SIAM Journal on Scientific Computing*, 28(1):303–320, 2006. doi:10.1137/040618953.

[47] R. Patterson, J. Singh, M. Balthasar, M. Kraft, and W. Wagner. Extending stochastic soot simulation to higher pressures. *Combustion and Flame*, 145(3):638–642, 2006. doi:10.1016/j.combustflame.2006.02.005.

[48] P. Penttinen, K. Timonen, P. Tiittanen, A. Mirme, J. Ruuskanen, and J. Pekkanen. Ultrafine particles in urban air and respiratory health among adult asthmatics. *European Respiratory Journal*, 17(3):428–435, 2001.

[49] J. Pinto da Costa, R. Cracknell, N. Seaton, and L. Sarkisov. Towards predictive molecular simulations of normal and branched alkane adsorption in carbonaceous engine deposits. *Carbon*, 49(2):445–456, 2011. doi:10.1016/j.carbon.2010.09.041.

[50] W. Piock, G. Hoffmann, A. Berndorfer, P. Salemi, and B. Fusshoeller. Strategies towards meeting future particulate matter emission requirements in homogeneous gasoline direct injection engines. *SAE International Journal of Engines*, 4(1):1455–1468, 2011. doi:10.4271/2011-01-1212.

[51] S. Pope. PDF methods for turbulent reactive flows. *Progress of Energy and Combustion Science*, 11:119–192, 1985. doi:10.1016/0360-1285(85)90002-4.

[52] A. Raj, M. Celnik, R. Shirley, M. Sander, R. Patterson, R. West, and M. Kraft. A statistical approach to develop a detailed soot growth model using PAH characteristics. *Combustion and Flame*, 156(4):896–913, 2009. doi:10.1016/j.combustflame.2009.01.005.

[53] E. Rivera, N. Mastro, J. Zizelman, J. Kirwan, and R. Ooyama. Development of injector for the direct injection homogeneous market using design for six sigma. *SAE Technical Paper 2010-01-0594*, 2010. doi:10.4271/2010-01-0594.

[54] M. Rossbach, A. Velji, U. Wagner, U. Spicher, R. Suntz, and H. Bockhorn. Investigations of the formation and oxidation of soot inside a direct injection spark ignition engine. *The spark ignition engine of the future, Strasbourg INSA*, 2009.

[55] C. Schwarz, E. Schünemann, B. Durst, J. Fischer, and A. Witt. Potentials of the spray-guided BMW DI combustion system. *SAE Technical Paper 2006-01-1265*, 2006. doi:10.4271/2006-01-1265.

[56] J. Senda, M. Kobayashi, S. Iwashita, and H. Fujimoto. Modeling of diesel spray impingement on a flat wall. *SAE Technical Paper 941894*, 1994. doi:10.4271/941894.

[57] L. Shih and D. Assanis. Implementation of a fuel spray wall interaction model in KIVA-II. *SAE Technical Paper 911787*, 1991. doi:10.4271/911787.

[58] Y. Shim, G. Choi, and D. Kim. Numerical and experimental study on effect of wall geometry on wall impingement process of hollow-cone fuel spray under various ambient conditions. *International Journal of Multiphase Flow*, 35(10):885–895, 2009. doi:10.1016/j.ijmultiphaseflow.2009.06.004.

[59] A. Smallbone, A. Bhave, A. Coble, S. Mosbach, M. Kraft, and R. McDavid. Identifying optimal operating points in terms of engineering constraints and regulated emissions in modern diesel engines. *SAE Technical Paper 2011-01-1388*, 2011. doi:10.4271/2011-01-1388.

[60] A. Smallbone, A. Coble, A. Bhave, S. Mosbach, M. Kraft, N. Morgan, and G. Kalghatgi. Simulating PM emissions and combustion stability in gasoline/diesel fuelled engines. *SAE Technical Paper 2011-01-1184*, 2011. doi:10.4271/2011-01-1184.

[61] Y. Sogawa, H. Hattori, T. Yamashita, N. Yanagisawa, T. Ikeda, S. Tanaka, M. Hosoya, K. Takahashi, T. Shoji, T. Suzuki, Y. Iwakiri, T. Nakajima, and Y. Tonegawa. Nano particle emission evaluation of state of the art diesel aftertreatment technologies (DPF, urea-SCR and DOC), gasoline combustion systems (lean burn/stoichiometric DISI and MPI) and fuel qualities effects (EtOH, ETBE, FAME, aromatics and distillation). *SAE Technical Paper 2007-01-4083*, 2007. doi:10.4271/2007-01-4083.

[62] D. Stanton and C. Rutland. Modeling fuel film formation and wall interaction in diesel engines. *SAE Technical Paper 960628*, 1996. doi:10.4271/960628.

[63] E. Stevens and R. Steeper. Piston wetting in an optical DISI engine: Fuel films, pool fires, and soot generation. *SAE Technical Paper 2001-01-1203*, 2001. doi:10.4271/2001-01-1203.

[64] B. Stojkovic, T. Fansler, M. Drake, and V. Sick. High-speed imaging of OH* and soot temperature and concentration in a stratified-charge direct-injection gasoline engine. *Proceedings of the Combustion Institute*, 30(2):2657–2665, 2005. doi:10.1016/j.proci.2004.08.021.

[65] H. Su, A. Vikhansky, S. Mosbach, M. Kraft, A. Bhave, K. Kim, T. Kobayashi, and F. Mauss. A computational study of an HCCI engine with direct injection during gas exchange. *Combustion and Flame*, 147(1-2):118–132, 2006. doi:10.1016/j.combustflame.2006.07.005.

[66] H. Su, S. Mosbach, M. Kraft, A. Bhave, S. Kook, and C. Bae. Two-stage fuel direct injection in a diesel fuelled HCCI engine. *SAE Technical Paper 2007-01-1880*, 2007. doi:10.4271/2007-01-1880.

[67] S. Subramaniam and S. Pope. A mixing model for turbulent reactive flows based on Euclidean minimum spanning trees. *Combustion and Flame*, 115(4):487–514, 1998. doi:10.1016/S0010-2180(98)00023-6.

[68] Y. Sukegawa, K. Kumano, and K. Ogata. Estimation of particulate matter in direct injection gasoline engines by non-combustion CFD. *SAE Technical Paper 2014-01-1142*, 2014. doi:10.4271/2014-01-1142.

[69] M. Trujillo, W. Mathews, C. Lee, and J. Peters. Modelling and experiment of impingement and atomization of a liquid spray on a wall. *International Journal of Engine Research*, 1(1):87–105, 2000. doi:10.1243/1468087001545281.

[70] A. Velji, K. Yeom, U. Wagner, U. Spicher, M. Rosbach, R. Suntz, and H. Bockhorn. Investigations of the formation and oxidation of soot inside a direct injection spark ignition engine using advanced laser-techniques. *SAE Technical Paper 2010-01-0352*, 2010. doi:10.4271/2010-01-0352.

[71] D. Wang and A. Watkins. Numerical modeling of diesel spray wall impaction phenomena. *International Journal of Heat and Fluid Flow*, 14(3):301–312, 1993. doi:10.1016/0142-727X(93)90062-R.

[72] A. Watkins and D. Wang. A new model for diesel spray impaction on walls and comparison with experiment. *International Symposium COMODIA*, 90:243–248, 1990.

[73] J. Welty, C. Wicks, R. Wilson, and G. L. Rorrer. *Fundamentals of Momentum, Heat, and Mass Transfer*. Wiley, New Jersey, 5th edition, 2008.

[74] Ł. Wyszyński, R. Aboagye, R. Stone, and G. Kalghatgi. Combustion imaging and analysis in a gasoline direct injection engine. *SAE Technical Paper 2004-01-0045*, 2004. doi:10.4271/2004-01-0045.